Fusion Reactor Design

Summary Report

By:
L. Angermann, J. Bancalari, E. Buglione-Ceresa, D. Corrias, L. Drescher, J. Francis, T. Gaggl, F. Halbwedl, D. Hipp, V. Keusch, D. Mendonça, M. Narnhofer, N. Oberth, M. Oblak, M. Prayer, J. Predigkeit, M. Steiner Michael, E. Steinwender, S. Strobl, M. Tritthart, F. Unterkofler, E. Wallner

Supervised by:
C. Albert, G. Birkenmeier, R. Schennach, J. Schilling, U. Stroth

September 4, 2024

Contents

1 Introduction

The following report documents the progress and intermediate results of "Fusion Reactor Design", a joint course between Graz University of Technology and the Technical University of Munich, supported by Proxima Fusion. It consists of a student project where the goal is to design a fusion reactor with stellarator geometry, with priority given to the following properties:

- **Size**: The reactor should be able to fit through a small door, imposing an upper size limit of (190x90) cm.
- **Aspect ratio and plasma volume:** While there is no hard limit here, the stellarator should have a high plasma volume, and thus the aspect ratio should be as low as possible without compromising other properties (stability, alpha particle losses, island reduction).
- **Coil simplicity:** The coils should be possible for a group of students to understand and theoretically construct. Realistically, this means that the number of coils and, more importantly, the number of coil types, should be kept at a minimum.

To realize this, the participants were assigned to five groups corresponding to different aspects of the reactor, depending on areas of expertise. These aspects are: 1) Coils, 2) Design and Optimization, 3) Diagnostics, 4) Heating, and 5) Vacuum. The exact progress and results of each of the groups are presented in the dedicated chapters, with brief summaries given here.

The Coils team is responsible for the design of the magnetic field coils given a configuration by the design team. Here, the main concerns lie in the coil materials, insulation and design, all while retaining proper spacing such that the configuration can fit into the vacuum chamber.

The Design and Optimization team provides the first coil configuration and optimizes parameters such as alpha losses and the iota profile, with the goal of stability against coil construction errors and deformations. Additionally, a 3D printed model is designed.

The Diagnostics team researches and proposes configurations of various measurement methods for verification of the magnetic field inside the reactor. Here, the methods include a) interferometry, b) Langmuir probe and c) Rogowski coil and d) diamagnetic coil.

The Heating team examines possible heating systems, specifically 2.45 GHz microwave technology, based on costs and whether it fits into the reactor. This is done by analyzing temperature and frequency profiles (the latter for both underdense and overdense plasma).

The Vacuum team is tasked with designing a functional vacuum chamber satisfying the size requirements while being able to contain all aforementioned parts. It should be capable of withstanding ultra high vacuum pressures, radiation and elements required to create the plasma.

Over the course of the semester, these teams have worked together to achieve a basic concept for a full design, which has potential to be built given proper time and funding.

2 Coils

2.1 Requirements and Tasks

The coils should be able to produce a magnetic field of $B = 87\,\mathrm{mT}$ and need to be able to fit into a vacuum-vessel with an inner diameter of $d_o = 1.6\,\mathrm{m}$ and a height of $h = 0.6\,\mathrm{m}$. The design and optimization team specified that the coil configuration should consist of a total of 12 coils with 3 unique coil types. The coil configuration provided by the design team should look like Figure 1. If possible, the coils should be able to sustain the continuous operation of

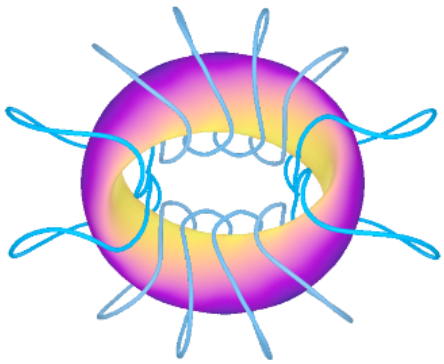

Figure 1: Coil configuration- taken from [1]

the Stellarator. During the cleaning of the vacuum chamber through heating the coils must withstand a temperature of at least 200 °C for a prolonged period of time. Furthermore the design of the coils must ensure that the vacuum is not contaminated by any adhesives or materials used. The generated magnetic field should have a desired deviation from the ideal field of less than 0.2 %. At last the design must also ensure that the system is collision free, to itself and other elements in the vacuum chamber, and in the realm of manufacturability for a student team. It follows from these requirements that the coils have to be manufactured very precisely, stiff and robust as well as mounted very precisely within the vacuum chamber.

2.2 Outcome

2.2.1 Structure

In order to meet the design requirements, the overarching structure of a coil is made up of a multitude of water cooled double pancake coils separated by a thin insulator material. The whole coil structure is then embedded into a steel casing in order to avoid contamination of the vacuum from the used adhesives and material combinations.

2.2.2 Manufacturing

It was determined early on that a costly and hard to manufacture solution on the basis of superconductors is not necessary and should be avoided. Due to the large power losses and the requirement of continuous operation cooling must to be considered. The most straightforward way of ensuring proper cooling is a water-cooling solution. To accommodate the water-cooling, the conductor within the coil has to have a hollow cross-section that is big enough to allow for good water flow and heat transport. Two options to manufacture such a hollow conductor were investigated:

- 3D printing the complete coil pack out of copper
- Copper pipes bent into the required coil geometries

While 3D printers can achieve high purity prints, with effective conductivities being close to 99% of pure copper, current manufacturing methods do not allow us to print the geometries in the necessary dimensions and with a suitable internal surface smoothness. The internal roughness is of special concern, since water has to flow through the windings without too much pressure loss. Additionally the powder used during manufacturing remains in the channels and can be difficult to remove from the manufactured coils. Due to this it was decided to use conventional manufacturing methods. While the manufacturing of the complex geometries might prove challenging for future teams, the advantages of off the shelf copper conductors, especially high performance conductors, cannot be overstated. As mentioned above the coils are designed to be inside a casing, which addresses both outgassing concerns, a well as the feedthroughs for water and current. For the casing of the coils, electron beam sintering could be considered in addition to 5-axis milling in order to achieve the necessary accuracy. The casings are flanged to the walls of the vacuum chamber, such that the inside of the casings are not under vacuum, which makes the design of the winding pack easier.
(for more: "Isolation and 3D Printing" PowerPoint presentation).

2.2.3 Insulation

The windings within a coil have to be insulated from each other. The best option seems to be fibre glass reinforced epoxy, as it can be bought in pre-impregnated rolls and further improves stability. The epoxy has to be hardened for which the coil might have to cooled, using the already in place water-cooling. Then the epoxy can withstand the applied temperature and forces and it should be around 0.5 mm to 1.0 mm thick. In order to prevent outgassing of the coils into the vacuum chamber, they are to be enclosed with a stainless steel casing of 2.0 mm thickness, which could either be 3D printed or manufactured by arc welding sheet metal.

2.2.4 Optimization

A python script was developed in order to explore the space of possible configurations. In the beginning rough estimates for the magnetic field and size were used, later they were replaced by the actual currents supplied by the optimization team and the size of the vacuum chamber. The overall goal was to reduce both power loss and pressure loss, while staying within some reasonable bounds for voltage and current. This was done for different winding configurations and pipe diameters. Figure 2 shows an example output. The simulation is based on double pancakes, meaning, that two neighbouring coils are paired and supplied with water separately.

A design with rectangular pipes and circular holes for water greatly improves the power loss and pressure loss characteristics. While these pipes exist and are used for high current applications, it is unclear if there are suppliers which could be contacted. (for more see Github)
In order to validate these results an experiment was designed. However, due to problems with the delivery of equipment, the test has not yet been conducted.

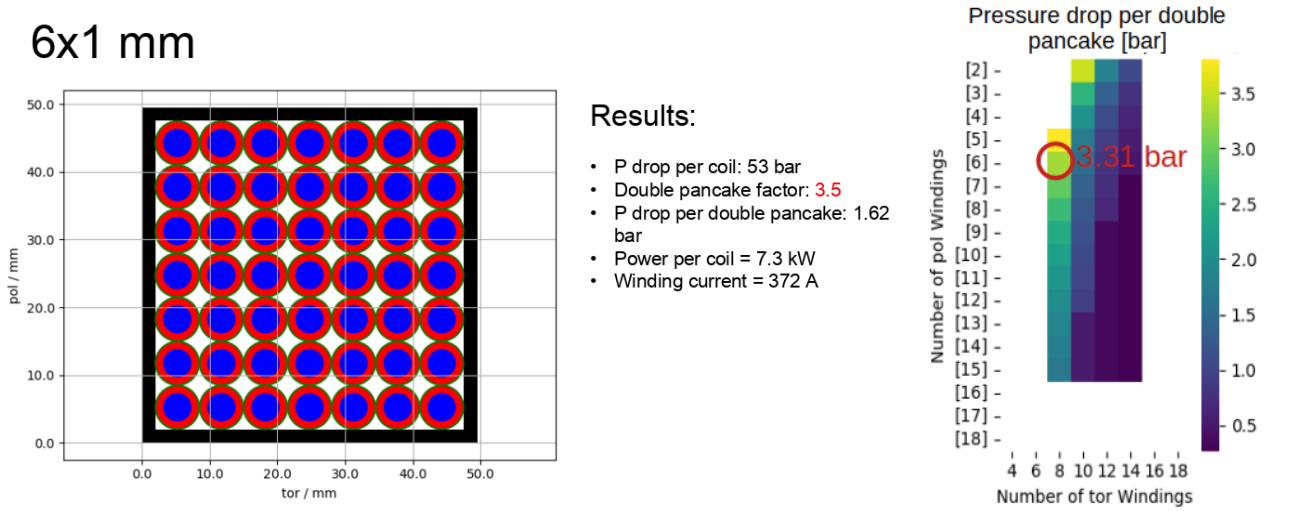

(a) Coil cross-section of 7x7 windings.

(b) Pressure drop

Figure 2: (6x1) mm pipe configuration and (6x1) mm pipe pressure drop calculation for different configurations

2.2.5 3D Modeling

The filaments, created by the optimization team, have been imported into Autodesk Fusion 360. However, the program was not able to process the actual extrusion process, as especially constructed coordinate systems had to be used in order to ensure the coils are not touching. For this purpose Python and CadQuery were used. Furthermore, Python scripts for the determination of the maximum dimension as well as the minimum distance between coil filaments were created. This was then also used to determine the scaling factor for the optimization teams data (it was set to be 0.33). Due to collisions of the coil, the final coil cross-section was set to (40x67) mm.

A mount for the coils was conceptually drawn and constructed in Autodesk Fusion as can be seen in figure 3. It enables the coils to be mounted to the vacuum chamber and for them to be adjusted and aligned from outside the chamber. Additionally it serves as port for the electrical cables and the water hoses. In order to allow for movement through the walls of the vacuum chamber a bellow has to be used.

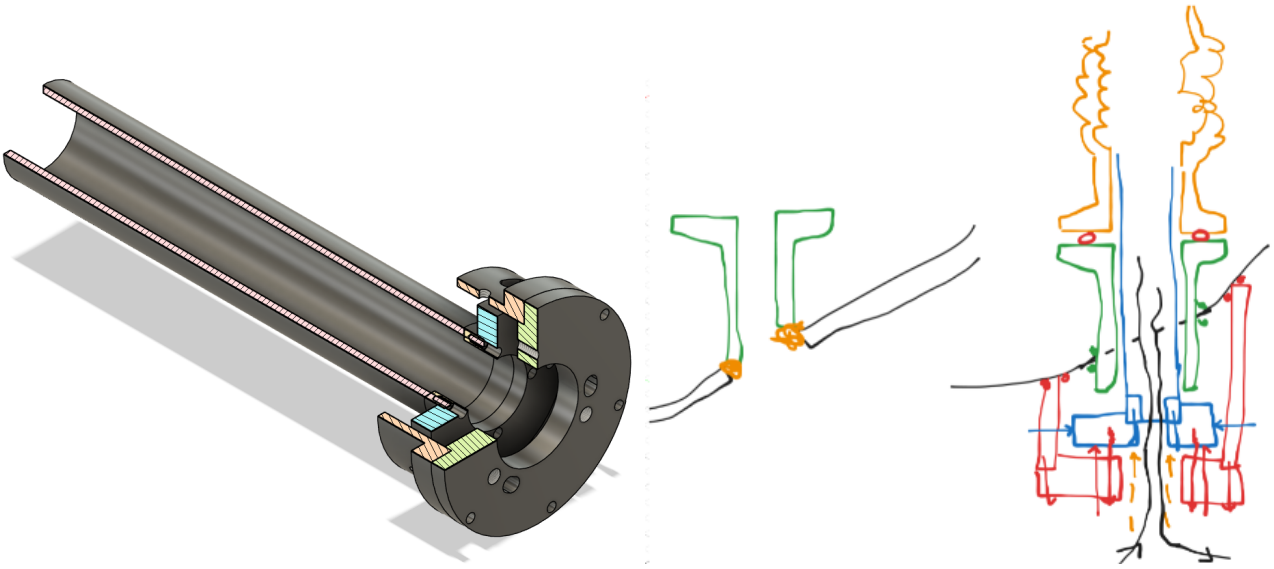

Figure 3: Coil Mount and principle. The left picture shows the modelled manipulator, which allows for precise alignment of the coils. The right pictures show a sketch of the attachment scheme.

To calculate both magnetic fields and Lorentz forces between coils, another python script was written. It also enable the calculations of moments, in the center of mass of the coils. The forces due to the magnetic fields were found to be much weaker than the ones due to gravity, which is why it was decided to mount the coils directly over there center of gravity, without any additional reinforcement. Figure 4 shows the deformation due the expected forces along the mounting mechanism.

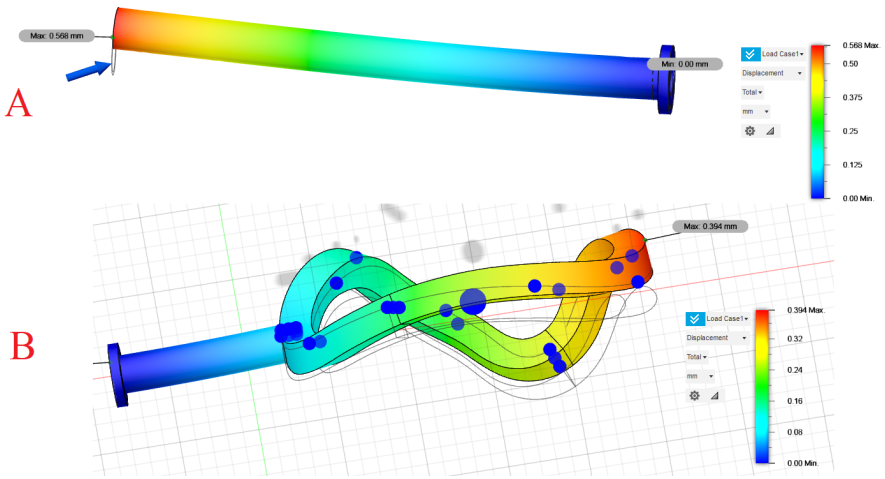

Figure 4: A: the deformation of a steel tube with 80 cm (approximated distance of coil center of mass to attachment point). B: the deformation of a full coil model, with forces still acting in the center of mass.

2.3 Outlook

The following points can be seen as next steps:

- The experimental verification of the design space model has to be completed.
- The manufacturing process of the coils has to be examined in greater detail.
- Further detailing of the CAD models has to be done.
- The magnetic and structural behaviour of the coils should be validated via detailed Multiphysics FEM simulation. This simulation has to take in account that the coils are essentially composites with an inhomogeneous and anisotropic behaviour.
- Further refining of the CAD Model and creation of 2D drawings for manufacturing.

2.4 Learnings

One big revelation is how difficult it is to draw the CAD Model and that Fusion 360 is not capable of such complex operations. This comes from the complicated filament geometry. Another challenge was to model the transition between each winding. One of the bigger challenges connected to this was to find a local coordinate system for which the coils do not collide and also do not deform too much.

3 Design

3.1 Requirements and Tasks

Design a reactor small enough to fit through a door. The magnetic (vacuum) field of the reactor should be "small and fat", in this case meaning a large volume with a small aspect ratio. Additionally, a minimal possible number of unique coil types should be achieved for ease of manufacturing. The design must be scalable in a way such that the minimum inter-coil distance for the model does not subceed 15 mm.

3.2 Outcome

After searching the QUASR data base it was decided that [1], a design with 3 distinct coil types and an aspect ratio of about 4 shall serve as the base, with the possibility of further optimizations being performed on it using SIMSOPT, STELLOPT, and SIMPLE (for alpha particle tracing). Table 1 shows the calculated alpha particle losses for certain magnetic flux surfaces, both for the small model and a scale-up.

Table 1: Confined alpha particle fraction on certain magnetic flux surfaces sbeg for one specific run of SIMPLE, for both the small model as well as a model scaled to the plasma volume of Wendelstein 7-X.
sbeg... Flux surface on which the particle tracing starts
c_f... Confined fraction of the plasma remaining after 10 ms
$c_{f,\text{scaled}}$...confined fraction of a scaled up system $B_{fac} = 5$, $R_{fac} = 11.13$)

sbeg	c_f	$c_{f,\text{scaled}}$
0.1	0.63	0.85
0.2	0.56	0.77
0.3	0.54	0.77
0.4	0.49	0.76
0.5	0.46	0.72
0.6	0.41	0.71
0.7	0.42	0.75
0.8	0.43	0.71
0.9	0.35	0.69

An exemplary plot of Poincaré slices for the (not further optimized) vacuum field in case of a shifted coil can be seen in Figure 5.

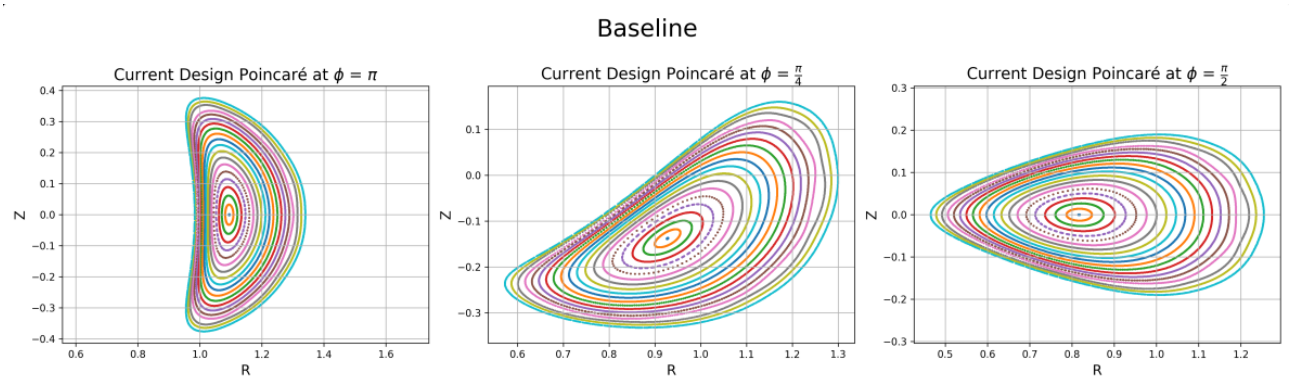

(a) Baseline/unshifted coils

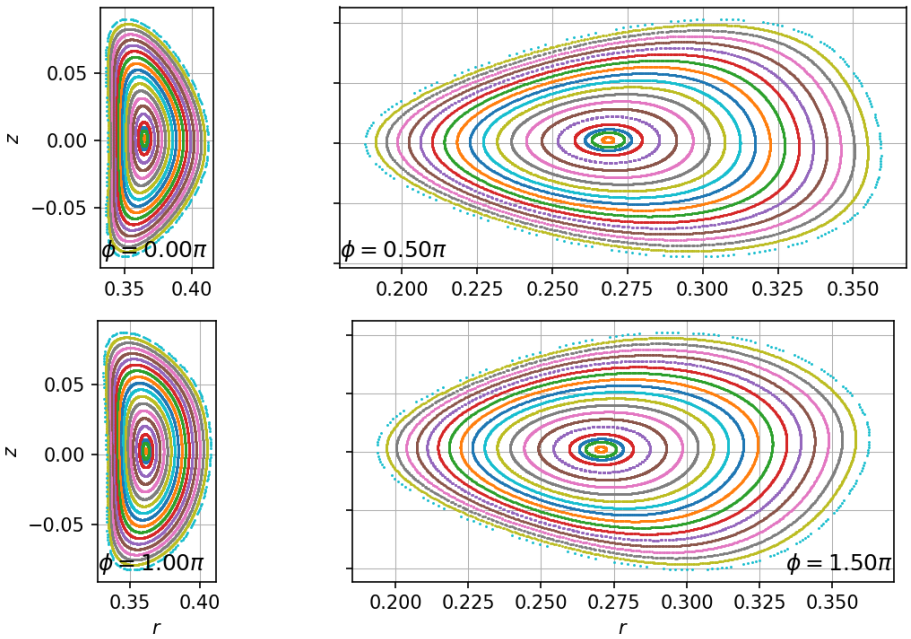

(b) One coil shifted by 1 cm.

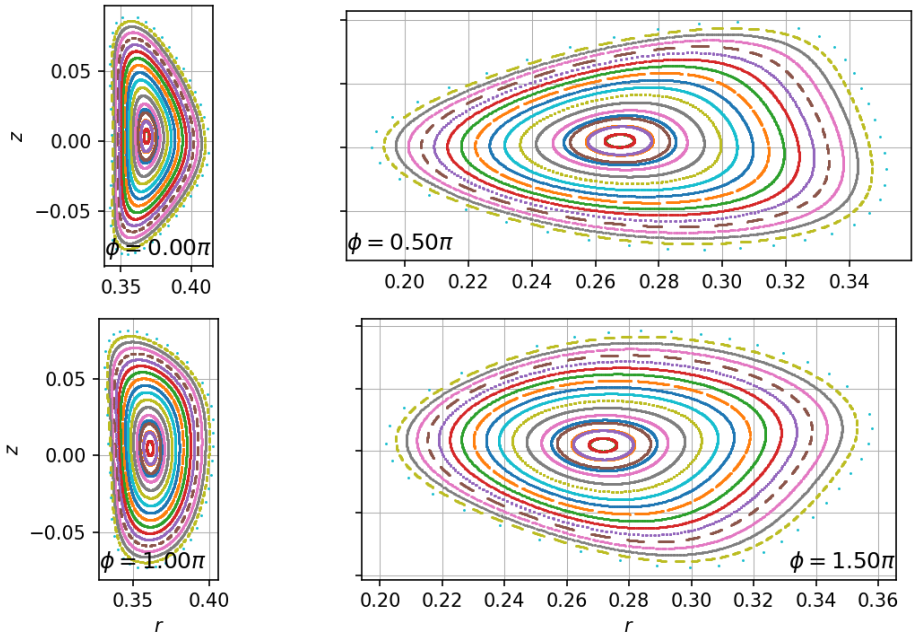

(c) One coil shifted by 2 cm.

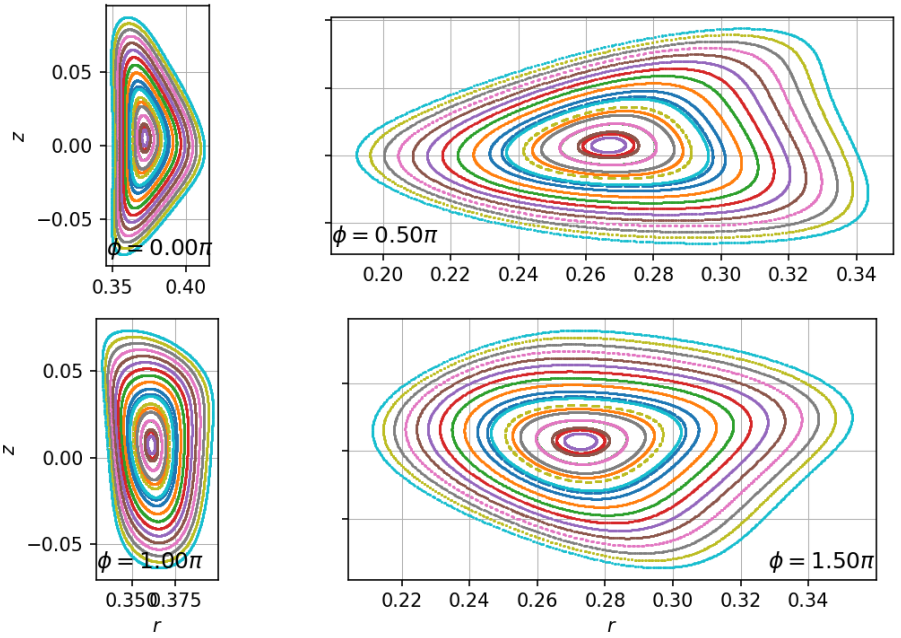

(d) One coil shifted by 3 cm.

Figure 5: Poincare plots for the fields of a) unshifted coils, b), c), d) one coil shifted.

Further results on the influence of manufacturing and positioning errors of the coils can be found at this Github repository [2].

3.3 Outlook

Further optimization could yield an even lower aspect ratio. One must take note of the coil shape however, as the inter-coil distance of the design refers to infinitesimally thin coils, meaning one

must leave enough space for a real world coil which in turn must be able to provide a magnetic field. Continuing to optimize the ι parameter towards a steeper profile (similar to LHC) or flatter (similar to W7X) profile may also be of interest to improve stability against errors.

3.4 Learnings

Even if small disturbances seem to have disastrous consequences for the vacuum field, the real world application will not be affected as much due to plasma fields. Theory results have much more pessimistic outcomes than the actual experiment.
Additionally, if scaled to "proper" reactor sizes, the model performs much better than the small version with a major radius of about 0.33 m. For example, the confined alpha particle fraction after 0.1 s calculated via SIMPLE goes from around 40% for the small reactor to around 70%. See Table 1.

4 Diagnostics

Diagnostics are needed to validate the calculated magnetic field as well as measure the densities and currents. For this, the diagnostics team designed an interferometer, a 2D-manipulator for the Langmuir probe in the y-z-direction, with a changeable probe tip, a fluorescence rod, a concept for a Rogowski coil measurement, concept for a diamagnetic coil measurement and a price comparison for different types of lock-in amplifier for a low temperature stellarator which has a configuration of $B = 87$ mT, $n_e < 10^{18}$ m^{-3} and $T_e = 10$ eV.

4.1 Requirements and Tasks

The interferometer measures the change in phase of a wave due to the plasma and relates it with the line integrated electron density of the plasma. First the maximum magnetic field and density need to be known, see above, to determine the maximum electron cyclotron and electron plasma frequency. Then it was shown that when a wave is sent into a magnetized plasma in such a way that the direction of propagation is perpendicular to the magnetic field, the ordinary wave, which has an oscillating electric field parallel to the magnetic field has a an index of refraction of $N = \sqrt{1 - \frac{\omega_{\mathrm{pe}}^2}{\omega^2}}$. This means that the wave needs to be sent in at a right angle to the magnetic field and with a frequency higher than the electron plasma frequency, which for our values is 9 GHz. When writing the resulting phase shift as a function of the frequency, the simplification that $\omega \gg \omega_{\mathrm{pe}}$ was used, meaning a frequency $f \gg 9$ GHz. Using Gaussian beams it was possible to derive the optimal dimensions of the mirror reflecting the wave. It is based on the frequency used and the distance between horn antenna and mirror which depends on the plasma diameter. Depending on the geometry of the vacuum vessel the horn antenna, which sends the wave, as well as the horn antenna that receives the reflected wave, can be placed inside the vacuum chamber. For this the geometry and the space available inside the chamber need to be known to calculate the positions of the horn antenna as well as the reflecting mirror.

The magnetic diagnostics has to extract the plasma currents out of a large background noise. In this project, the magnetic diagnostics consists of two diamagnetic coils, one Rogowski coil, and signal processing equipment. The diamagnetic coils measure the poloidal plasma current. The Rogowski coil measures the toroidal plasma current. The signal processing equipment consists of several lock-in amplifiers, low- and band-passes and D/A converters. They filter out the background noise, and amplify the plasma current signals.

For the Langmuir probe it is needed to scan the cross-section of the plasma to measure the $I - V$-characteristic of the plasma. With this characteristic plasma parameters are fitted (the floating potential Φ_{fl}, the plasma potential Φ_{p}, the electron current I_{e}, the ion current I_{i}, the electron saturation current $I_{\mathrm{e,sat}}$, the ion saturation current $I_{\mathrm{i,sat}}$ and the electron plasma density n_{e}).

In the left image of Figure 6 we can see that the electron saturation current has different curve shapes for different probe tips, for example for a spherical, cylindrical or a flat tip. The flat tip has the *sharpest* bend of all the tip geometries. The floating potential is the root of the $I - V$-characteristic, which occurs when the ion current and electron current are equal, negating each other resulting in zero current. The saturation currents exists because when the probe is charged one way, for example positive, all electrons in a region around the probe fly towards the probe. However, due to Debye shielding the created depletion region cannot grow

indefinitely. Once it reaches its maximum the current saturates and only thermal electrons outside the region enter the probe. The corresponding voltages are the plasma potential and the floating potential. With following equation the current of the probe can be determined:

$$I = I_i + I_e = enS\sqrt{\frac{T_e}{2\pi m_e}}\left[0.61\sqrt{\frac{2\pi m_e}{m_i}} - \exp\left\{-\frac{e(\Phi_p - U)}{T_e}\right\}\right] \tag{1}$$

$$I^*_{e,sat} = I_{e,sat}\left[1 + \frac{e(U - \Phi_p)}{T_e}\right]^{\gamma_{om}} \tag{2}$$

where $\gamma_{om} = 1/2$ is for cylindrical probe tips and $\gamma_{om} = 1$ is for spherical probe tips. [3]

4.2 Outcome

Having evaluated the basic parameters for the interferometer the schematic of the circuit was designed. The difficulty lies in measuring a phase shift occurring at a GHz frequency. For this purpose mixing the signals with a Gunn diode ring modulator is used to function as a down-converter. The local oscillator (LO) is run with a frequency ω and the reference oscillator (RO) with the frequency $\omega + \Delta\omega$, see the right image of Figure 7. With two mixers and amplifiers and band-pass filters we manage to get a signal with the frequency $\Delta\omega$. When we use a $\Delta\omega$ in the MHz range we can detect the phase shift with a phase detector. If there is not enough space inside the vacuum space an alternative design with Teflon lenses was also explored, see [4]. A python script was written with which one can calculate the ideal distances for every geometry and frequency.

Reagrding the Rogowski coil, the basic principles of the coil were explored. The diamagnetic effect in linear pinches was shortly reviewed, and different options regarding the lock-in amplifiers were examined. Simple CAD-models of the Rogowski and diamagnetic coils were created.

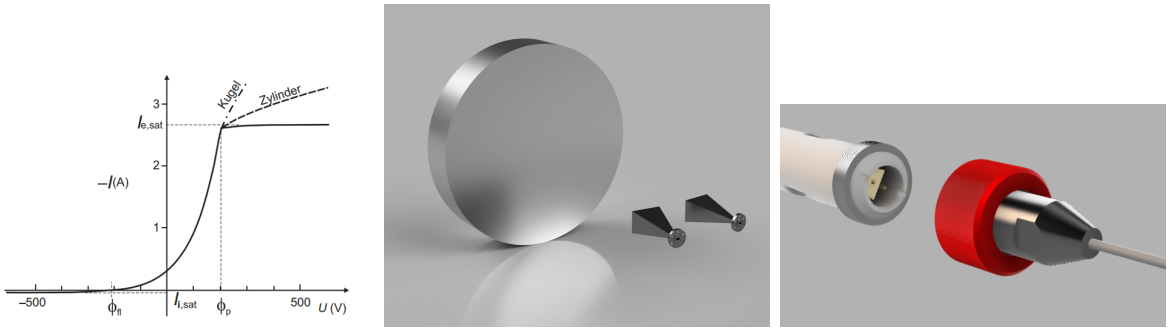

Figure 6: Left: I-V-characteristic of a Langmuir probe [3]. Middle: plasma CAD of the interferometer for a certain frequency and distance. Right: 3D-model of the changeable probe tip with a union nut.

The outcome at the Langmuir measurement was the geometry of the Langmuir probe tip which has a radius of 0.125 mm, a probe tip made out of tungsten, an isolation layer of aluminum oxide with the dimension of outer diameter of 1 mm and a inner diameter of 0.5 mm, a designing concept of a 2D-manipulator for the Langmuir measurement and the design of a changeable probe tip. Also the position and the geometry for the flange (DN400 ISO-F) at the vacuum vessel was determined. Additionally, a design of the small vacuum chamber for the manipulator

was created. It includes a power feed-through, a ball valve, a UHV slider to get a closed chamber for maintenance. Inside of the chamber there is a sliding system in three dimension to get a $z - y$-movement for the probe. The slinding bearings are made of iglidur®, because the use of any type of lubricant in the vacuum area is not recommended and this material absorbs little moisture. The left image of Figure 7 shows the 3D-model of the 2D-manipulator and the changeable probe tip.

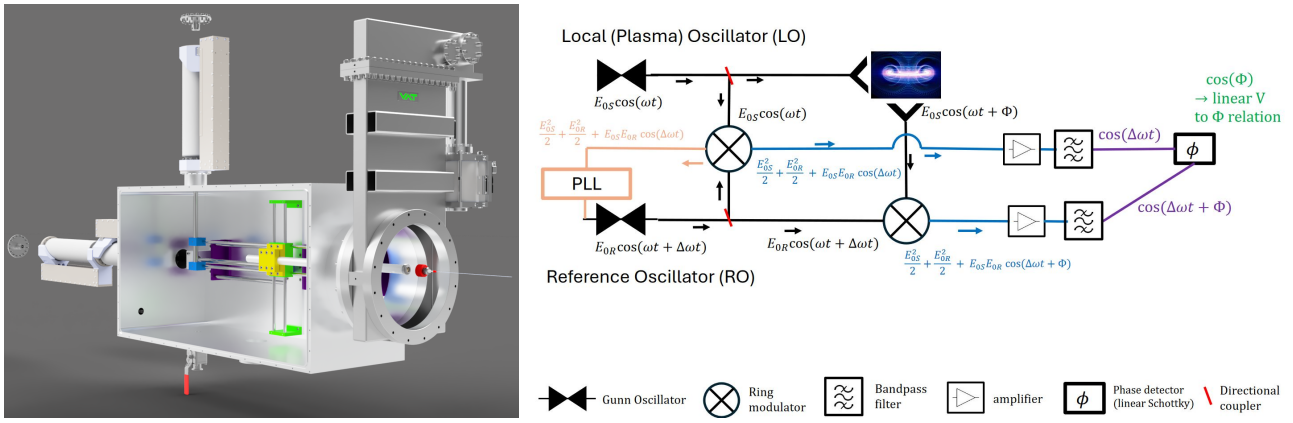

Figure 7: Left: 3D-model of the 2D-manipulator with a Langmuir probe. Right: Schematic of the circuit of the interferometer.

The outcome at the measurement of the magnetic flux lines was to design a fluorescence rod which has a coating of zinc-oxide (ZnO:Zn). The design for the rod was implemented to the changeable probe holder which has the same plug. Also an electron gun was designed.

4.3 Outlook

Gather together with electric/electronic staff of other teams to centralize power supply/signal processing. Further explicate requirements for signal processing equipment. Refine the preliminary CAD models of the Rogowski and diamagnetic coil. After deciding an oscillator with a certain frequency once can fix the geometry of the mirror and work on the mounting of the mirror. Similarly the circuit can be refined and the powers and voltages can be calculated. Finally, the appropriate hardware can be looked into and acquired. The observation window can be used for passive spectroscopy and additional diagnostics tools could also be designed to compliment the current instruments. It is necessary to choose the right material and a possible wall thickness for the vacuum chamber of the 2D-manipulator and the dimension. To design a 1000 mm manipulator for the 2D-manipulator on the side. The evaluation of the measurement and implement to LabVIEW. Designing an electron gun.

4.4 Learnings

Some basic properties of a static plasma configurations were learned. Concepts behind the lock-in technique were reviewed. Great difficulties were encountered in using the Autodesk Fusion CAD software. In order to understand the interferometer we learned plasma wave physics as well as the propagation of a wave in a waveguide and in the horn antenna. Furthermore we learned about signal processing, however we did not have much experience in that regard so we are still not sure if we chose the ideal circuit or if there are complications we have not thought of. A new 3D-CAD software and implement movements in the assembly group. Design movement

parts in vacuum and use the right bearings. Design layout of different plasma measurement systems. Concepts behind the Langmuir probe measurement and the measuring of a closed magnetic flux field. Cross-team collaboration.

5 Heating

5.1 Requirements and Tasks

To heat up the atoms to achieve a plasma and arrive at temperatures useful for experimentation, it is necessary to add a heating system to the reactor. It was known already before that heating equipment using 2.45 GHz microwave technology is probably the cheapest. But it had to be elaborated if it can be fitted to the reactor, and what the price point is. Also, it had to be verified, that the method is working for the parameters of the reactor to be built. One more goal was to determine the parameters that could be achieved by means of the heating scheme.

5.2 Outcome

5.2.1 Power balance

To validate whether 2.45 GHz heating will work, the density profiles had to be determined. Those profiles, alongside the temperature profiles, were also of interest to get a glimpse of the parameters that the reactor will achieve upon successful implementation.
From a preliminary 0D simulation implemented as described in [5], it became clear that the lower the neutral density n_{neu}, the lower the achievable electron densities. Another outcome was that the higher the heating power, the higher the input density.

A 1D simulation, using the approach described in [6], was then performed. Here, the major difference was, that the the plasma parameters were a function of the minor radius r. Although the results presented here are at equilibrium, the 1D simulation also allows to calculate the profiles over time during the start phase. This is not used here since this would require to change the heating profile.

For the diffusivities and neutral densities, the parameters from the TJ-K experiment in Stuttgart were used, as shown in Table 2.

Table 2: 1D simulation parameters.
D ... particle diffusivity
χ ... heat diffusivity
n_new ... neutral density

	Helium	Argon
D / $\mathrm{m^2\,s^{-1}}$	8.5	6
χ / $\mathrm{m^2\,s^{-1}}$	200	8
n_{new}	2.30×10^{18}	2.32×10^{17}

Figure 8 shows the resulting temperature and density profiles, assuming that all the heating power can be deposited into the plasma without losses. The profiles for Helium have the same shape, but the maximum temperature is 47 eV instead of 32 eV, and the maximum density is $0.58 \times 10^{18}\,\mathrm{m^{-3}}$ instead of $1.23 \times 10^{18}\,\mathrm{m^{-3}}$.

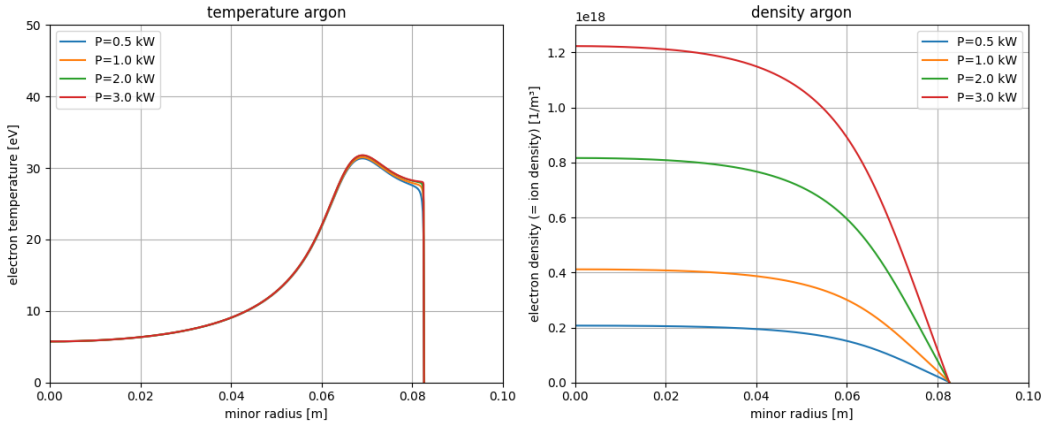

Figure 8: 1D equilibrium radial profiles for Argon.

One interesting outcome is that the temperature profile seems to be almost independent from the heating power. This can be explained by the fact that at the heating profile, there is an equilibrium between newly ionized particles and "lost" particles due to diffusion (towards the plasma core and towards the plasma edge). For this, one should take into account the average time τ that an ion spends in the heating zone before floating away due to diffusion. As soon as the average power deposited per particle per dwell time τ reaches the ionization energy, ionization will dominate, taking away all the excess energy. Only below 100 W, the temperature begins to sink when reducing the heating power further.

Also, the gradient at the outer edge is probably steeper than it would be in the experiment. Here, the reason is likely that the diffusion profiles taken from [6] are for temperatures around 10 eV instead of 30 eV, and therefore too low for the presented machine.

5.2.2 Heating processes

In order to recreate how the heating would occur, a series of theoretical approximations were made. To start with, even though this is a design of a stellarator, a toroidal symmetry was assumed. Then, the density profile was assumed to be parabolic and poloidally centred and the magnetic field to decay with $1/r$. It was also assumed that the frequency of the wave sent into the plasma was much higher than the ion cyclotron (IC) frequency ($\omega >> \omega_{ci}$), so the dynamics of the ions, which are much slower than the electrons, was overall neglected.

The interest is to have an overdense plasma, $\omega_{pe} > \omega_{ce}$ everywhere, making it impossible to heat up the plasma only by exciting the electron cyclotron resonance (ECR). This is because the incoming wave will be reflected at the critical density, where the wave reaches ω_{pe}. There will also have to be excitation of the upper-hybrid resonance (UHR), but, when plasmas are overdense, the R-wave that permits this heating method is also reflected back at the ω_R cut-off before reaching this mode. These frequency profiles can be seen in Figure 9. In the end, a combination of these heating processes, alongside with O-X-B heating will be necessary in order to heat up the plasma. The O-X-B process consists of having an O-wave ($\overrightarrow{E_1} // \overrightarrow{B_0}$) propagate into the plasma until being reflected at ω_{pe} and converted into an X-wave ($\overrightarrow{E_1} \perp \overrightarrow{B_0}$). In turn, this X-wave propagates in the direction contrary of emission until being reflected back again at ω_R and converted into a Bernstein wave. This wave can finally cross through the ω_{pe} cut-off frequency and reach the position in the plasma where ECR heating (ECRH) can occur. In practice, however, we expect the heating radiation to disperse throughout the vacuum vessel,

being reflected off of the walls (and having its polarity change) and absorbed through various other processes.

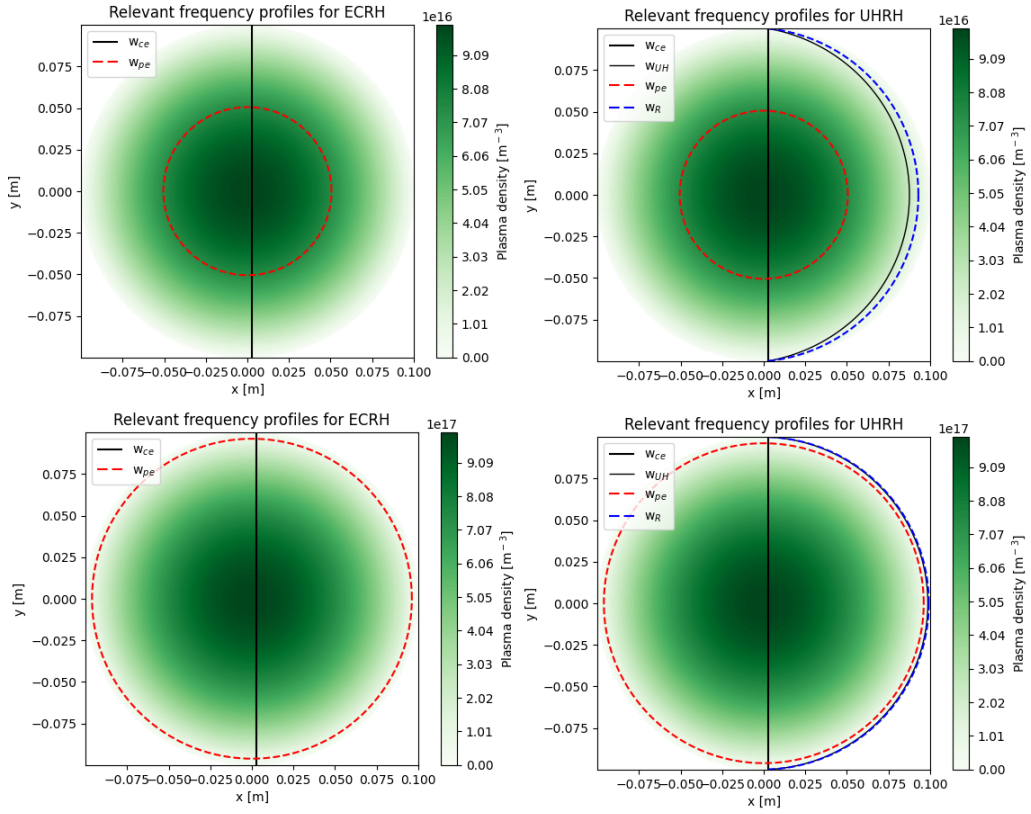

Figure 9: Frequency profiles for ECRH and UHRH for non overdense (top) and overdense (bottom) plasma. The resonant frequencies ω_{ce} and ω_{UH} and the cut-off frequencies ω_{pe} and ω_R are displayed.

5.2.3 Hardware

The 2.45 GHz microwaves will be generated by a magnetron, and transported to the plasma by WR340 waveguides (86.36 x 43.18) mm. This size was chosen to maintain polarization by only allowing the TE1 mode to propagate. Upon reaching the vacuum chamber, the microwaves will be focused using an optimum horn antenna. It is important for effective heating, that the wider H-plane flare is oriented along the vertical axis perpendicular to the containment B-field. Further RF components must be added along the waveguides to minimize feedback into the magnetron. A circulator and a directional coupler are added to remove any returning waves. A 3-stub tuner is added before the horn antenna to maximize the heating system's efficiency.

5.3 Outlook

In the end, further developments can still be made. In regard to the cross-sectional wave resonance and cut off profiles, only the example of a tokamak was studied. This was enough to understand what will qualitatively happen, upon heating of the plasma, but the quantitative study is not applicable to a stellarator design. Further work on this could then consist of figuring out which cross section of the stellarator is most ideal to perform heating on, depending on its shape.

5.4 Learnings

One of the main learnings from the simulations were that the major two parameters to achieve are higher densities are heating power, but also the neutral density n_{new}. A more technical learning was, that while [6] employed the Crank-Nicelson scheme for numerical implementation, a naïve fully-explicit scheme works as well. The only downside was, that around 500 times more steps were needed. But the python/numpy-based implementation still took less than 5 minutes per case (depending on number of radial points).

6 Vacuum

6.1 Requirements and Tasks

The main task of the vacuum team is to design a vacuum chamber that can be used for a small table top stellarator. For this the maximum size of the chamber was given, so it can fit through a standard door of (90 x 200) cm. Thus this are the maximum dimensions of the individual parts of the chamber.

The necessary requirements for the chamber are: (a) The chamber should be large enough to fit the coils for the stellarator as well as all other devices to generate and measure the plasma, (b) needs to be able to withstand pressures $< 10^{-8}$ mbar, when evacuated, (c) should be able to encounter different types of noble gases to create the plasma, (d) should be able to withstand the radiation of the plasma as well the microwave radiation of the heating.

In order to achieve these requirements, the focus is on the design of the vacuum chamber, the vacuum system, and the radiation protection. This is described in more detail in the full *Vacuum Team Report*. This report also includes the design process, description of the most important ports and feedthrough, the vacuum system, and the radiation protection. Here only a brief overview of the most important1 aspects is given.

6.2 Outcome

6.2.1 Vacuum chamber

The design of the vacuum chamber, which was finalized, is shown in Figure 10. It has a dome shaped lid as well as a dome shaped base. This allowed to increase the size of the chamber as the base and the lid are both removable and can be placed together inside a laboratory. The given specifications of the size were given, that the chamber need to fit through a standard door, with the size of (90 x 200) cm. Also other configuration were considered, for example with a flat base and a flat lid, but the dome shaped design was chosen as it was the most rigid one. The rigidity is needed to prevent the chamber from bending when evacuated to a pressure of $< 10^{-8}$ mbar.

For the sake of simplicity, all flange connections were chosen to have the same size. Only the connections for the Pirani-Bayard-Alpert pressure measurement and the quadrupole spectrometer were chosen differently, as little was previously known of specific flange sizes. The universal fange connections chosen for the versatile connection is the same flange used as for the TMP (DN 320 ISO-F). This flange size was chosen because if a second TMP is needed, it can be easily added to the chamber using a knee. Also the relative large size of the flange allows to connect other flanges to it using adapters.

Apart from the ports already known for the chamber, additional ports with standard flanges are added. This makes is easier for the future use of the chamber, as retrofitting extra ports is not necessary. Also adding ports from the beginning makes it cheaper, as not much work is needed to add them later on.

To support the wight of the chamber, foots are added to the side of the vessel. This will allow to place the entire chamber on a steel scaffold. Thus, these mounts need to be able to support the entire weight of the chamber as well as the weight of the external mounted devices.

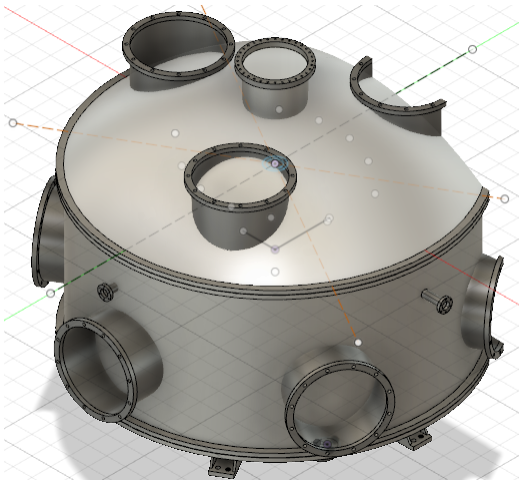

(a) Final version of the vacuum chamber.

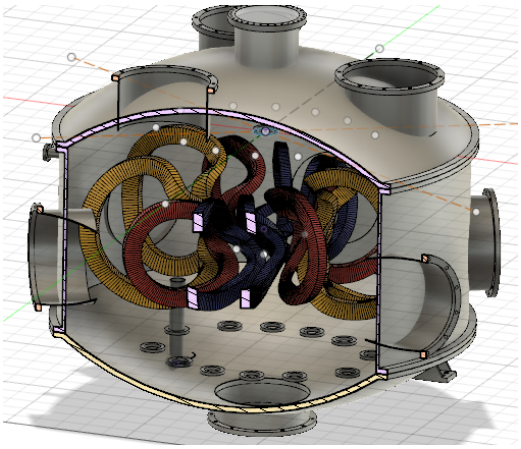

(b) Sectional analysis of the chamber: The flanges for the coil connections facing inwards are visible on the inside.

Figure 10: Views of the completed vacuum chamber at the status of the 10.07.2024.

6.2.2 Vacuum design

For the Vacuum system a turbo-molecular pump is chosen, due its oil-free operation and pumping speed. It is backed up by a sufficiently sized backing pump which also provides the rough vacuum before the TMP takes over. To reduce outgassing metal surfaces in the inside are polished and wires are heat and electrically isolated by using e.g. Kapton®. Pressure is measured using a pressure gauge that includes a Pirani device for lower vacuum levels and a Bayard-Alpert device for higher vacuum ranges. For a residual gas analysis one port is reserved for hosting a quadrupole mass spectrometer.

6.2.3 Radiation protection

The vacuum vessel is designed with a thickness of 10 mm, which provides adequate protection against X-ray and microwave radiation. The chosen material is austenitic stainless steel 316L. This material was selected due to its non-magnetic nature and its advantageous properties, including high strength, good availability, and overall versatility, making it an ideal choice for our application.

The window was designed with a circular shape having a radius 100 mm made of quartz glass. The ideal thickness for the window is 10 mm.

6.3 Outlook

It is important to perform a detailed structural analysis to ensure the chamber can withstand external atmospheric pressure and any mechanical stresses without significant deformation or failure. Moving forward, the design of the vacuum chamber may need to be adjusted based on the specific requirements of the other teams involved in the design process. The exact number and types of ports, as well as other components such as windows, gas inlets, feedthroughs, and coaxials, have not been finalized yet. Therefore, additional work will be needed to finalize these details and to ensure that the vacuum chamber design meets all necessary requirements. It is also necessary to ensure that the design meets relevant safety standards and regulations for vacuum systems and radiation protection. Safety features such as emergency shutdown systems

and radiation monitoring should be included. For this reason, integration of various sensors and instrumentation for monitoring temperature, radiation levels and other critical parameters should be considered. Moreover, it is essential to develop safety protocols for handling and maintenance, ensuring personnel are aware of and protected from potential radiation exposure. At this stage, the cost of the vacuum chamber itself remains unknown and cannot be estimated. The manufacturer does not provide list prices for such custom-made items and would only provide a cost estimate upon specific order inquiry. It is anticipated that the vacuum chamber itself would represent one of the largest expenses for the entire project, primarily due to the necessity of custom manufacturing.

6.4 Learnings

Designing the vacuum chamber for a small stellarator has provided significant insights into project management. This includes conducting independent research and efficiently integrating findings into our design decisions. Recognizing the importance of considering diverse perspectives and requirements from other teams involved was both challenging and instructive. Collaborating closely with other teams emphasized the importance of sharing skills and expertise, resulting in a more cohesive project outcome.

7 Conclusion

In 2024, the joint course *Fusion Reactor Design* was held for the first time in a partership of TGraz University of Technology, Technical University of Munich and Proxima Fusion GmbH. The Coils, Design, Diagnostics, Heating and Vacuum teams have each contributed and worked together to design and provide a concept for a small stellarator magnetic plasma confinement experiment in each of their respective fields of expertise. The requirements decided at the beginning of the project were prioritized and are conceptually fulfilled: 1) Size limit of (190x90) cm, 2) low aspect ratio of around 4, and 3) few (three) different coil types. As a final result, a CAD model with all the components contributed by the various teams is available.

As with any project of this complexity, there are various areas of possible improvement. On the theoretical end, more simulations to verify the coil structure, as well as continued optimization to improve general design stability and lowering the aspect ratio, could be performed. Additionally, refinement of the diagnostics circuits, study of the heating design for the complexities of a stellarator and structural and safety analysis of the vacuum chamber are further possibilities.

Because the practical/experimental portion had lower priority in this project, it is essentially open end. The specific materials and suppliers for construction of the coils and vacuum chamber have been considered, but not finalized, and of course there is 1) the actual construction and 2) the experimental verification of the functionality of the entire design. Given the funding and time (possible future semesters), these would be highly interesting future continuation options for the project.

Acknowledgements

This work has been carried out within the framework of the EUROfusion Consortium, funded by the European Union via the Euratom Research and Training Programme (Grant Agreement No 101052200 — EUROfusion). Views and opinions expressed are however those of the author(s) only and do not necessarily reflect those of the European Union or the European Commission. Neither the European Union nor the European Commission can be held responsible for them. We thank Max-Planck-Institute for Plasma Physics, in particular the team of Eve Stenson. We gratefully acknowledge support from NAWI Graz, Proxima Fusion, and TU Graz via the seed funding and Joint Course initiatives.

References

[1] Andrew Giuliani. *Flatiron Institute QUAsi-symmetric Stellarator Repository*. URL: https://quasr.flatironinstitute.org/model/0021326.

[2] *Fusion Reactor Design 2024 central Github repository*. https://github.com/itpplasma/reactor24.

[3] Ulrich Stroth. *Plasmaphysik*. Berlin, Heidelberg: Springer Berlin Heidelberg, 2018. ISBN: 978-3-662-55235-3. DOI: 10.1007/978-3-662-55236-0.

[4] D. H. Choi et al. "Design of interferometer system on Versatile Experiment Spherical Torus (VEST) at Seoul National University". In: *Journal of Instrumentation* 7.1 (Jan. 2012), p. C01107. DOI: 10.1088/1748-0221/7/01/C01107.

[5] Carsten Lechte, Jennifer Stöber, and Ulrich Stroth. "Plasma parameter limits of magnetically confined low temperature plasmas from a combined particle and power balance". In: *Physics of Plasmas* 9.6 (June 2002), pp. 2839–2846. ISSN: 1070-664X. DOI: 10.1063/1.1467928. eprint: https://pubs.aip.org/aip/pop/article-pdf/9/6/2839/19097666/2839_1_online.pdf. URL: https://doi.org/10.1063/1.1467928.

[6] Gregor Birkenmaier. *Experiments and Modeling of Transport Processes in Toroidal Plasmas - Diploma Thesis*. Stuttgart, 2008.

List of Figures

List of Tables